Heterogeneous clinical phenotypes and cerebral malformations reflected by rotatin cellular dynamics

Vandervore, Laura V; Schot, Rachel; Kasteleijn, Esmee; Oegema, Renske; Stouffs, Katrien; Gheldof, Alexander; Grochowska, Martyna M; van der Sterre, Marianne L T; van Unen, Leontine M A; Wilke, Martina

Published in:
Brain

DOI:
10.1093/brain/awz045

Publication date:
2019

doi:10.1093/brain/awz045 BRAIN 2019: 142; 867–884 | 867

BRAIN
A JOURNAL OF NEUROLOGY

Heterogeneous clinical phenotypes and cerebral malformations reflected by rotatin cellular dynamics

Laura V. Vandervore,[1,2,3] Rachel Schot,[1] Esmee Kasteleijn,[1] Renske Oegema,[1,‡] Katrien Stouffs,[2,3] Alexander Gheldof,[2,3] Martyna M. Grochowska,[1] Marianne L.T. van der Sterre,[1] Leontine M.A. van Unen,[1] Martina Wilke,[1] Peter Elfferich,[1] Peter J. van der Spek,[4] Daphne Heijsman,[1,4] Anna Grandone,[5] Jeroen A.A. Demmers,[6] Dick H.W. Dekkers,[6] Johan A. Slotman,[7] Gert-Jan Kremers,[7] Gerben J. Schaaf,[1,8] Roy G. Masius,[1] Anton J. van Essen,[9,*] Patrick Rump,[9] Arie van Haeringen,[10] Els Peeters,[11] Umut Altunoglu,[12] Tugba Kalayci,[12] Raymond A. Poot,[13] William B. Dobyns,[14,15] Nadia Bahi-Buisson,[16] Frans W. Verheijen,[1] Anna C. Jansen[2,3,17] and Grazia M.S. Mancini[1]

*Deceased.

See Uzquiano and Francis (doi:10.1093/brain/awz048) for a scientific commentary on this article.

Recessive mutations in *RTTN*, encoding the protein rotatin, were originally identified as cause of polymicrogyria, a cortical malformation. With time, a wide variety of other brain malformations has been ascribed to *RTTN* mutations, including primary microcephaly. Rotatin is a centrosomal protein possibly involved in centriolar elongation and ciliogenesis. However, the function of rotatin in brain development is largely unknown and the molecular disease mechanism underlying cortical malformations has not yet been elucidated. We performed both clinical and cell biological studies, aimed at clarifying rotatin function and pathogenesis. Review of the 23 published and five unpublished clinical cases and genomic mutations, including the effect of novel deep intronic pathogenic mutations on *RTTN* transcripts, allowed us to extrapolate the core phenotype, consisting of intellectual disability, short stature, microcephaly, lissencephaly, periventricular heterotopia, polymicrogyria and other malformations. We show that the severity of the phenotype is related to residual function of the protein, not only the level of mRNA expression. Skin fibroblasts from eight affected individuals were studied by high resolution immunomicroscopy and flow cytometry, in parallel with *in vitro* expression of *RTTN* in HEK293T cells. We demonstrate that rotatin regulates different phases of the cell cycle and is mislocalized in affected individuals. Mutant cells showed consistent and severe mitotic failure with centrosome amplification and multipolar spindle formation, leading to aneuploidy and apoptosis, which could relate to depletion of neuronal progenitors often observed in microcephaly. We confirmed the role of rotatin in functional and structural maintenance of primary cilia and determined that the protein localized not only to the basal body, but also to the axoneme, proving the functional interconnectivity between ciliogenesis and cell cycle progression. Proteomics analysis of both native and exogenous rotatin uncovered that rotatin interacts with the neuronal (non-muscle) myosin heavy chain subunits, motors of nucleokinesis during neuronal migration, and in human induced pluripotent stem cell-derived bipolar mature neurons rotatin localizes at the centrosome in the leading edge. This illustrates the role of rotatin in neuronal migration. These different functions of rotatin explain why *RTTN* mutations can lead to heterogeneous cerebral malformations, both related to proliferation and migration defects.

Received September 7, 2018. Revised November 26, 2018. Accepted January 7, 2019. Advance Access publication March 16, 2019

1 Department of Clinical Genetics, Erasmus University Medical Center (Erasmus MC), P.O. Box 2040, 3000 CA Rotterdam, The Netherlands
2 Neurogenetics Research Group, Research Cluster Reproduction, Genetics and Regenerative Medicine, Vrije Universiteit Brussel, Brussels, 1090, Belgium
3 Center for Medical Genetics, UZ Brussel, Brussels, 1090, Belgium
4 Department of Pathology, Clinical Bio-informatics, Erasmus University Medical Center (Erasmus MC), P.O. Box 2040, 3000 CA Rotterdam, The Netherlands
5 Dipartimento della Donna, del Bambino, di Chirurgia Generale e Specialistica, Seconda Università degli studi della Campania "L. Vanvitelli", Naples, Italy
6 Department of Molecular Genetics, Proteomics Center, Erasmus University Medical Center (Erasmus MC), P.O. Box 2040, 3000 CA Rotterdam, The Netherlands
7 Department of Pathology, Optical Imaging Center, Erasmus University Medical Center (Erasmus MC), P.O. Box 2040, 3000 CA Rotterdam, The Netherlands
8 Center for Lysosomal and Metabolic Diseases, Erasmus Medical Center (Erasmus MC), 3015 CN Rotterdam, The Netherlands
9 Department of Genetics, University of Groningen, University Medical Center Groningen, P.O. Box 30.001, 9700 RB, Groningen, The Netherlands
10 Department of Clinical Genetics, LUMC, Leiden University Medical Center, Postzone K-5-R, Postbus 9600, 2300 RC Leiden, The Netherlands
11 Department of Pediatric Neurology, Juliana Hospital, Els Borst-Eilersplein 275, 2545 AA Den Haag, The Netherlands
12 Department of Medical genetics, Istanbul Medical Faculty, Istanbul University, Topkapı Mahallesi, Turgut Özal Millet Cd, 34093 Fatih/İstanbul, Turkey
13 Department of Cell biology, Erasmus University Medical Center (Erasmus MC), P.O. Box 2040, 3000 CA Rotterdam, The Netherlands
14 Department of Pediatrics, University of Washington, Seattle, WA 98195, USA
15 Center for Integrative Brain Research, Seattle Children's Research Institute, Seattle, WA 98101, USA
16 Imagine Institute, INSERM UMR-1163, Laboratory Genetics and Embryology of Congenital Malformations, Paris Descartes University, Institut des Maladies Génétiques 24, Boulevard de Montparnasse, Paris, 75015, France
17 Pediatric Neurology Unit, Department of Pediatrics, UZ Brussel, Brussels, 1090, Belgium

‡Present address: Department of Genetics, University Medical Center Utrecht, The Netherlands

Correspondence to: Grazia M.S. Mancini
Department of Clinical Genetics, Erasmus University Medical Center, 3000 CA Rotterdam,
The Netherlands
E-mail: g.mancini@erasmusmc.nl

Correspondence may also be addressed to: Laura Vandervore
Neurogenetics Research Group, Laarbeeklaan 101, 1090 Brussels, Belgium
E-mail: Laura.Vandervore@vub.be

Keywords: *RTTN*; microcephaly; mitosis; centrosome amplification; MYH10

Introduction

The *in utero* development of the human cerebral cortex, starting at 8 weeks of gestation, is a complex process depending on different developmental steps including neurogenesis, neuronal migration, post-migrational organization and connectivity (Barkovich *et al.*, 2012; Guerrini and Dobyns, 2014). Interruption of any of these pathways may result in a malformation of cortical development, classically divided into disorders of neuronal proliferation (e.g. microcephaly or megalencephaly), neuronal migration (e.g. lissencephaly and neuronal heterotopia) and cortical organization (e.g. polymicrogyria). Autosomal recessive primary microcephaly (MCPH) is a cortical malformation characterized by a reduced brain size at birth with an occipitofrontal circumference of three standard deviations (SD) below the age- and sex-matched norm (Barkovich *et al.*, 2012; Faheem *et al.*, 2015). Multiple genes involved in pathways of mitotic spindle formation, centrosome and centriole duplication, DNA replication, repair and damage response have been linked to MCPH (Faheem *et al.*, 2015). Several processes regulating neuronal migration are linked to microtubule structure and function, including participation of centrosomes (the microtubule organizing centre) and primary cilia (microtubule-based sensory organelles) (Guemez-Gamboa *et al.*, 2014; Guo *et al.*, 2015; Romero *et al.*, 2018). In contrast, the mechanisms leading to cortical organization are heterogeneous and disorganization, as seen in polymicrogyria, has for example been associated with variants of tubulin genes, such as *TUBA1A* (OMIM#602529), *TUBB2B* (OMIM#612850), *TUBB3* (OMIM#602661) and *TUBB* (OMIM#191130) (Bahi-Buisson and Cavallin, 2016; Romero *et al.*, 2018).

Genetic alterations in rotatin, encoded by the *RTTN* (OMIM #610436) gene, were originally linked to autosomal recessive polymicrogyria in two families, but were later also

associated with primary microcephaly and primordial dwarfism in additional families (Kheradmand Kia *et al.*, 2012; Shamseldin *et al.*, 2015; Grandone *et al.*, 2016; Rump *et al.*, 2016; Vora *et al.*, 2017; Cavallin *et al.*, 2018; Chartier *et al.*, 2018; Stouffs *et al.*, 2018; Wambach *et al.*, 2018). Studies in human fibroblasts allocated rotatin to the basal body of the primary cilium, suggesting involvement of the protein in primary ciliogenesis and sonic hedgehog (SHH) signalling (Kheradmand Kia *et al.*, 2012; Wambach *et al.*, 2018). Further studies in the human cancer cell lines HeLa, KE37 and U2OS showed that the protein also localized to the centrosome in interphase and mitosis (Stevens *et al.*, 2009; Kheradmand Kia *et al.*, 2012; Chen *et al.*, 2017). *Rttn*$^{-/-}$ knockout mouse embryos fail to undergo axial rotation, neural tube closure, left-right specification, heart looping and are not viable (Faisst *et al.*, 2002; Chatterjee *et al.*, 2007). Stevens *et al.* (2009) studied the involvement of the *Drosophila melanogaster RTTN* homologue *Ana3* in centriole duplication, since *Ana3* depletion led to increased anastral spindles. Ana3 shows centrosomal localization distinct from centriole duplication mediator homologues for human polo-like kinase 4 (PLK4), SAS-6, CPAP, and STIL. Interestingly, many of these centriole duplication proteins have been previously linked to microcephaly.

The centrosome is a conserved eukaryotic organelle consisting of a pair of centrioles, an older mother and younger daughter procentriole, embedded in a pericentriolar matrix (Bettencourt-Dias *et al.*, 2011). Each centriole is composed of nine microtubule triplets, doublets or singlets (Stevens *et al.*, 2010). During G0 interphase, the centrosome migrates to the cell cortex where the mother centriole forms the basal body, nucleating the axoneme of the primary cilium (Stevens *et al.*, 2010; Bettencourt-Dias *et al.*, 2011). Preceeding cell division, in G1 or S phase, centrosome duplication takes place. A new procentriole is nucleated perpendicularly to each pre-existing centriole, and will elongate in S and G2 phases (Marthiens and Basto, 2014). During mitosis or M-phase, these two centrosomes form the spindle poles and direct the formation of bipolar mitotic spindles. The correct number of centrosomes during mitosis is essential for accurate chromosome segregation into daughter cells.

Ana3 mutant embryonic neuroblasts display an increase in the mean number of centrosomes per cell (centrosome amplification) (Stevens *et al.*, 2009). However, this is in contrast with loss of centriole duplication factors PLK4, SAS-6 and CPAP, leading to a decrease in the mean number of centrosomes per cell in *D. melanogaster* and human cells (Stevens *et al.*, 2009; Gambarotto and Basto, 2016).

Centrosome amplification during mitosis can lead to aneuploidy with multipolar spindle assembly, asymmetric cell division or multiple cilia formation (Bettencourt-Dias *et al.*, 2011). In human, variants in genes *MCPH1* (microcephalin 1, OMIM#607117), *CDK5RAP2* (MCPH3, OMIM#608201), *CDK6* (OMIM#603368), *STIL* (OMIM#181590) and *CEP135* (OMIM#611423) lead to centrosome amplification and are associated with microcephaly (Barrera *et al.*, 2010; Marthiens *et al.*, 2013; Arquint and Nigg, 2014; Marthiens and Basto, 2014; Gambarotto and Basto, 2016). CEP135 and STIL proteins have been proposed to interact with rotatin during the early phase of centriole elongation (Gupta *et al.*, 2015; Chen *et al.*, 2017).

Although evidence has been provided that rotatin is a centrosome-related protein, its role during the main events related to centriolar function, i.e. mitosis and ciliogenesis, is largely elusive. The fact that human *RTTN* variants have been described with heterogeneous cerebral malformations and clinical course, induced us to systematically review the clinical presentation and explore the protein function in mutant cells from several unrelated affected individuals.

Materials and methods

Cases

The study was approved by the local IRB of the Erasmus MC University Medical Center Rotterdam (protocol METC-2012387). Clinical data and material from affected individuals were recruited through collaboration within the European Network on Brain Malformations (Neuro-MIG, COST Action CA16118; www.neuro-mig.org). Written informed consent was obtained from all parents/caretakers. Fibroblasts from affected individuals were obtained from skin biopsies previously sampled for routine diagnostics. Further experimental procedures are provided in the Supplementary material.

Data availability

WES/WGS data are deposited internally at the Erasmus MC and in each medical institute referring the patients, in respect to the privacy of the families.

The mass spectrometry proteomics data have been deposited in the ProteomeXchange Consortium (Deutsch *et al.*, 2017) via the PRIDE (Vizcaíno *et al.*, 2016) partner repository with the dataset identifier PXD012415.

Results

Genetic alterations of *RTTN* in novel families

Germline variants in *RTTN* have been reported in 13 families, with a total of 23 affected individuals (Kheradmand Kia *et al.*, 2012; Shamseldin *et al.*, 2015; Grandone *et al.*, 2016; Rump *et al.*, 2016; Vora *et al.*, 2017; Cavallin *et al.*, 2018; Chartier *et al.*, 2018; Stouffs *et al.*, 2018; Wambach *et al.*, 2018). Here we report three additional families, including five affected individuals, and two novel recessive alterations in *RTTN*. Clinical reports of novel cases are summarized in the Supplementary material and Supplementary Table 7, and respective brain MRI images can be found in Fig. 1. We also included one family with two affected siblings, in which an *RTTN*

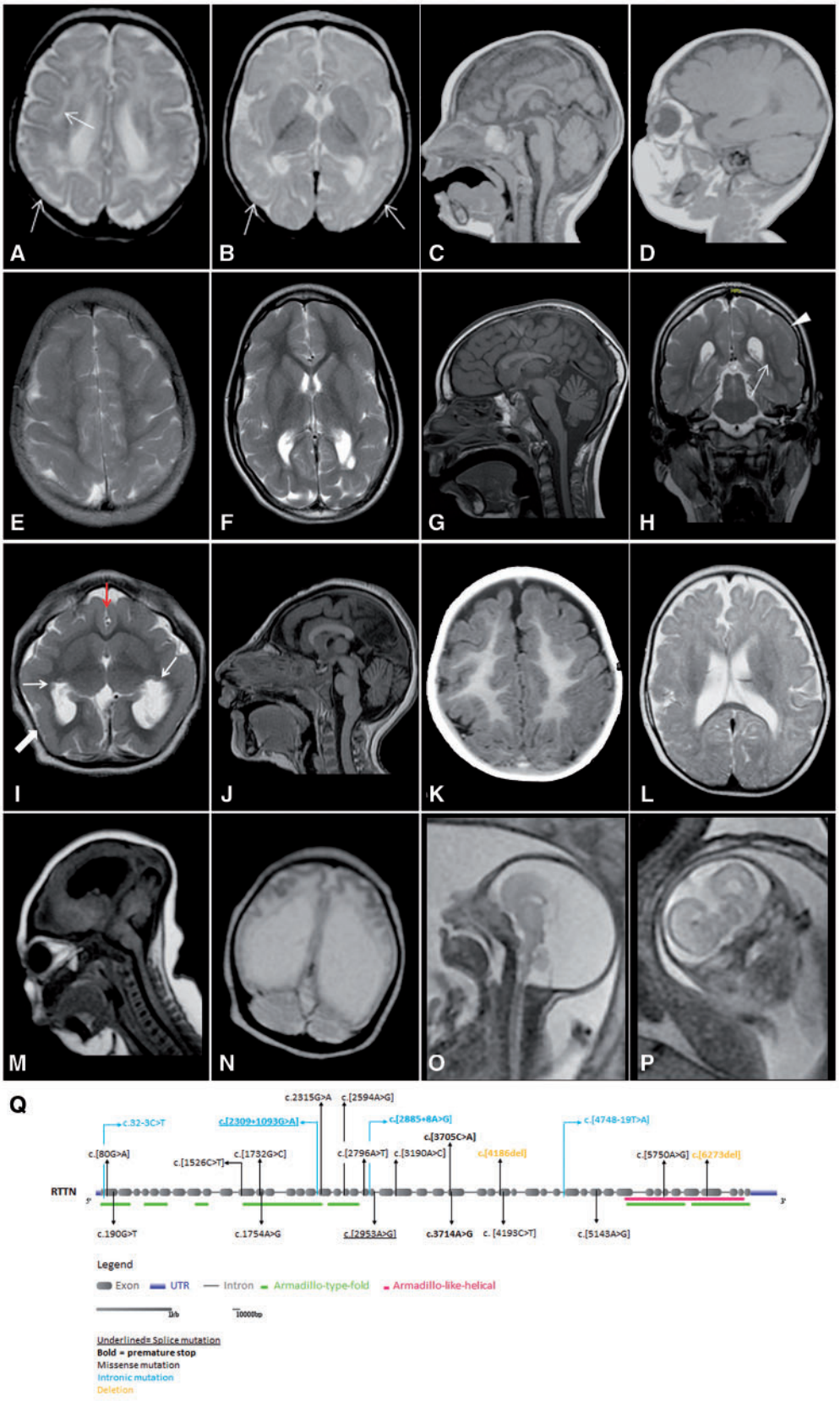

Figure 1 Brain MRI images from patients with biallelic *RTTN* mutations (A–P) and graphical overview of all *RTTN* mutations (Q). (**A**–**D**) Proband of Family A (P1) MRI at age 9 months. (**A** and **B**) T_2-weighted axial images showing diffuse simplified gyri and abnormal cortex with a suspected subcortical ribbon of neurons separated by a cell sparse zone (arrows), a modest anterior > posterior gradient, moderately enlarged occipital horns of lateral ventricles, normal basal ganglia. (**C** and **D**) Midsagittal and parasagittal T_1-weighted images showing

(continued)

mutation was described but for whom no clinical details were reported (Rump *et al.*, 2016).

In Family A, the compound heterozygous variants found in exon 20 and 31 of *RTTN* (c.[2594A>G];[4186del], p.[His865Arg];[Glu1397Lysfs*7], NM_173630.3) were discovered by exome sequencing during a microcephaly cohort screening and were reported previously (Rump *et al.*, 2016).

In Family B (Supplementary Table 7), homozygosity mapping (using Affymetrix 6.0 SNP arrays) identified regions of homozygosity in five chromosomes, comprising 309 genes in two affected sisters, which are not shared by their healthy brother. Whole genome sequencing was negative for coding homozygous pathogenic variants in regions of homozygosity. However, a candidate gene approach led by the phenotype identified a homozygous c.[2309+1093G>A] splice variant in intron 17 of *RTTN*, creating a new splice acceptor site at c.2309+1095. The variant does not appear in ExAC, dbSNP, ESP, GoNL and gnomAD databases (coverage for each analysis is shown in Supplementary Table 3).

In Family H, a homozygous variant c.[2953A>G] was found by whole exome sequencing, affecting the penultimate nucleotide in exon 23 of *RTTN*, identical to that reported in Families C and D (Grandone *et al.*, 2016; Cavallin *et al.*, 2018). Aberrant splicing was reported in Families C and D and verified in this study. The arginine at position 985 is highly conserved among different orthologues, although not located at an armadillo type fold domain of rotatin. All three families are Moroccan and consanguineous. This variant does not appear in the ExAC, dbSNP, ESP, GoNL and gnomAD databases.

In Family I, a compound heterozygous change was found by exome sequencing c.[3705C>A];[4748–19T>A]. The first paternal variant leads to a premature stop p.[Tyr1235*] in exon 28. The second maternal variant in intron 35 is predicted to lead to a novel splice acceptor site at position c.4748–17, which is predicted to lead to an insertion of 17 bp and a premature stop. Both variants did not appear in other genome databases (ExAC, dbSNP, ESP, GoNL, gnomAD).

Recessive variants in *RTTN* lead to a variable phenotypic spectrum

Following our report in 2012 of *RTTN* mutations in individuals with intellectual disability and cerebral polymicrogyria, additional subjects have been described with a different clinical presentation, including other brain malformations (primary microcephaly), growth defects and congenital anomalies (Kheradmand Kia *et al.*, 2012; Shamseldin *et al.*, 2015; Grandone *et al.*, 2016; Rump *et al.*, 2016; Vora *et al.*, 2017; Cavallin *et al.*, 2018; Chartier *et al.*, 2018; Stouffs *et al.*, 2018; Wambach *et al.*, 2018). The phenotypic spectrum that emerges after reviewing all clinical reports with bi-allelic *RTTN* variants has been summarized in Table 1 and shows that the most common, although not obligate, features are severe intellectual disability, lack of speech and primary microcephaly. Primordial dwarfism (defined as birth weight and length <2.5 SD for gestational age and gender) is common in microcephalic newborns. Cortical malformations have been observed in all individuals studied with brain imaging or at post-mortem. The spectrum is broad, ranging from polymicrogyria-like dysgyric cortex with borderline small head in milder cases, to severe congenital microcephaly with large interhemispheric cysts and CSF filling most of the skull, up to disruptive appearance of schizencephaly. The cortical malformation is often predominant in frontal regions, suggesting elective underdevelopment of frontal lobes (Fig. 1) (Cavallin *et al.*, 2018). Normal pressure hydrocephalus, prominent in *Rttn*$^{-/-}$ knockout mice, is also present in several individuals (Shamseldin *et al.*, 2015) (Family I, Supplementary Table 2). The clinical severity correlates with the extension of the migration disorder and with the extent of microcephaly, individuals with pachygyria and commissural dysgenesis being more severely affected than the ones with microcephaly and simplified gyri or polymicrogyric cortex and borderline microcephaly. As in mice, variable congenital anomalies of internal organs occur, particularly in the urogenital system, suggesting prominent involvement of the endo-

Figure 1 Continued

hypoplastic corpus callosum, pachygyric cortex and normal cerebellum. (**E**–**H**) Affected sister of P1 Family A, MRI at age 8 years. (**E** and **F**) T_2-axial images showing diffuse pachygyria with anterior > posterior gradient, enlarged occipital horns of lateral ventricles, normal basal ganglia, small intraparenchymal cyst in the left occipital horn. (**G**) Sagittal T_1 image showing thin hypoplastic corpus callosum. (**H**) Coronal T_2 image showing pachygyria of the temporo-parietal cortex, thin subcortical band of neurons parallel to the ventricular surface (arrow) and an apparent cell sparse area under the cortex (arrow head). (**I** and **J**) Proband of Family C (P3). MRI at 2 years, (**I**) axial T_2-weighted image showing a grey matter ribbon apparently bridging across the frontal hemispheres and seemingly fused basal ganglia (red arrow), nodular heterotopia (thin arrows) and temporo-parietal polymicrogyria (thick arrow). (**J**) Sagittal T_1-weighted image showing hypoplastic rostrum and splenium of corpus callosum with increased interhemispheric space. (**K** and **L**) Proband of Family F (P6) MRI at the age of 1 year. IR-T_1 and T_2-weighted images showing diffuse but asymmetric cortical dysgyria, with frontal predominance and enlarged ventricles, respectively. (**M** and **N**) Proband of Family H MRI at birth. (**M**) Sagittal T_1 showing severe enlarged ventricle and cortical dysgyria. (**N**) Coronal T_2 image showing ventriculomegaly and thin hypointense cortical layer, possibly microgyric. (**O**) T_2-weighted images MRI at the 27th week of gestation of proband 1 from Family I, showing large intracranial cyst and underdeveloped cortex. (**P**) T_2-weighted image MRI of proband 2, Family I, at 24th week of gestation, showing large interhemispheric cyst and underdeveloped cortex. (**Q**) Schematic overview of all reported and novel *RTTN* mutations with specified protein domains.

Table 1 Summary of *RTTN* mutation phenotypes in all published and novel cases reported herein

Disease manifestation	Number of individuals with *RTTN* alteration (n = 28)	Percentage of all assessed individuals
Growth parameters and survival		
Primary microcephaly (OFC < 2.5 SD at birth)	17/21 7 not known[a]: (Kheradmand Kia *et al.*, 2012; Shamseldin *et al.*, 2015; Wambach *et al.*, 2018), Family B	81%
Primordial dwarfism (length <2.5 SD at birth)	7/20 8 not known[a]: (Shamseldin *et al.*, 2015; Chartier *et al.*, 2018), Family B	35%
Pre-natal demise	5/28 terminated pregnancies Family I and Chartier *et al.*, 2018	18%
Postnatal early death	4/23 2 months (Shamseldin *et al.*, 2015), 17 days (Shamseldin *et al.*, 2015), 4 months (Wambach *et al.*, 2018) and 12 years (Rump *et al.*, 2016)	17%
Postnatal microcephaly[a]	7/23 (Kheradmand Kia *et al.*, 2012; Shamseldin *et al.*, 2015; Wambach *et al.*, 2018), Family B	30%
Postnatal short stature[a]	10/23 (Shamseldin *et al.*, 2015; Rump *et al.*, 2016; Stouffs *et al.*, 2018; Wambach *et al.*, 2018)	43%
Clinical features (n = 23)[b]		
Moderate/severe developmental delay, age >2 years	20/20	100%
No speech or few words. age >2 years	18/20 Except (Kheradmand Kia *et al.*, 2012; Rump *et al.*, 2016)	90%
Seizures	4/23 (Kheradmand Kia *et al.*, 2012; Wambach *et al.*, 2018), Family H	17%
Wheelchair-bound	1/20 (Family H)	5%
Independent walking (age)	8/20 (16 months–2.6 years) (Shamseldin *et al.*, 2015; Grandone *et al.*, 2016; Rump *et al.*, 2016; Stouffs *et al.*, 2018), Family B	40%
Congenital eye anomalies (micropthalmia, abnormal orbitae, ankyloblepharon, optic hypoplasia)	2/23 (Wambach *et al.*, 2018); Family H	9%
Congenital heart disease	3/23 Tetralogy of Fallot (Rump *et al.*, 2016), atrial septal defect (Grandone *et al.*, 2016)	13%
Kidney defect (agenesis, ectopy, pyelocaliectasis)	5/23 (Kheradmand Kia *et al.*, 2012; Shamseldin *et al.*, 2015; Rump *et al.*, 2016; Wambach *et al.*, 2018)	22%
Gastrointestinal (duodenal atresia)	1/23 (Shamseldin *et al.*, 2015)	4%
Urogenital system (cryptorchid-ism, micropenis, double uterus)	9/23 (Shamseldin *et al.*, 2015; Grandone *et al.*, 2016; Rump *et al.*, 2016; Wambach *et al.*, 2018), Family B and Family H	39%
Skin abnormality (congenital dermatitis)	4/23 (Grandone *et al.*, 2016; Rump *et al.*, 2016; Stouffs *et al.*, 2018)	17%
Skeletal congenital anomalies (kyphoscoliosis, hip dysplasia)	4/23 (Rump *et al.*, 2016; Stouffs *et al.*, 2018), Family B	17%
MRI (n = 23)[c]		
Simplified gyration	10/23 (Shamseldin *et al.*, 2015; Chartier *et al.*, 2018; Wambach *et al.*, 2018) and Families H and I	43%
Lissencephaly/pachygyria	11/23 (Shamseldin *et al.*, 2015; Grandone *et al.*, 2016; Rump *et al.*, 2016; Cavallin *et al.*, 2018; Stouffs *et al.*, 2018) and Families H and I	48%
Polymicrogyria/dysgyria NOS/schizencephaly	7/23 (Kheradmand Kia *et al.*, 2012; Shamseldin *et al.*, 2015; Cavallin *et al.*, 2018; Stouffs *et al.*, 2018) and Family I	30%
Nodular heterotopia	6/23 (Shamseldin *et al.*, 2015; Grandone *et al.*, 2016; Cavallin *et al.*, 2018; Chartier *et al.*, 2018) and Family H	26%
Subcortical band heterotopia	1/23 (Rump *et al.*, 2016)	4%
Suspected holoprosencephaly	2/23 (Shamseldin *et al.*, 2015; Cavallin *et al.*, 2018)	9%
Other midline developmental defect (aplasia of olfactory bulbs, hypoplastic CC)	15/23 (Kheradmand Kia *et al.*, 2012; Shamseldin *et al.*, 2015; Grandone *et al.*, 2016; Rump *et al.*, 2016; Vora *et al.*, 2017; Stouffs *et al.*, 2018) and Families H and I	65%
Interhemispheric posterior arach-noid cyst	4/23 (Grandone *et al.*, 2016; Vora *et al.*, 2017) and Family I	17%
(Ponto)cerebellar hypoplasia	7/23 (Kheradmand Kia *et al.*, 2012; Shamseldin *et al.*, 2015; Grandone *et al.*, 2016; Vora *et al.*, 2017; Wambach *et al.*, 2018)	30%

[a]In these individuals no OFC or length at birth was recorded.
[b]No additional features mentioned in five terminated pregnancies and in features where was specified (>2 years of age), n = 20 since three patients died in infancy.
[c]Permission denied from Family B, Family F oldest sister 5, and Family I V:3 and V:41.
CC = corpus callosum; OFC = occipitofrontal circumference; NOS = not otherwise specified.

crine/pituitary system. Eye globes, orbits and eyelid abnormalities are relatively frequent in severe cases (9% of total), which together with the underdevelopment of the frontal lobes, the frequent occurrence of midline defects (65%) and signs of pituitary failure (growth and endocrine anomalies), indicates, besides dorsal, also maldevelopment of ventral telencephalon.

RTTN mRNA expression and rotatin protein in cells from affected individuals

We were able to obtain and investigate cultured skin fibroblasts from eight affected individuals, here indicated as P1 [proband 1 from Family A (Rump *et al.*, 2016)], P2 (proband 1 from Family B), P3 [proband 1 from Family C (Cavallin *et al.*, 2018)], P4 [Family D (Grandone *et al.*, 2016)], P5 [Family E (Kheradmand Kia *et al.*, 2012)], P6 [Family F (Kheradmand Kia *et al.*, 2012)], and P7 and P8 [probands 1 and 2 from Family G (Stouffs *et al.*, 2018)], belonging to seven families. Quantitative reverse transcription-polymerase chain reaction (RT-qPCR) (Fig. 2A) or RT-PCR (Supplementary Fig. 1) of *RTTN* mRNA in these fibroblasts was carried out.

With RT-qPCR, residual *RTTN* transcript could be detected in cells from all affected individuals. P1–P3 showed a significant decrease in *RTTN* mRNA expression (Fig. 2A). P1 presents a compound heterozygote variant c.[2594A > G];[4186del] leading to p.His865Arg and p.Glu1397Lysfs*7 and shows the lowest expression of *RTTN* mRNA. Sanger sequencing of *RTTN* mRNA in

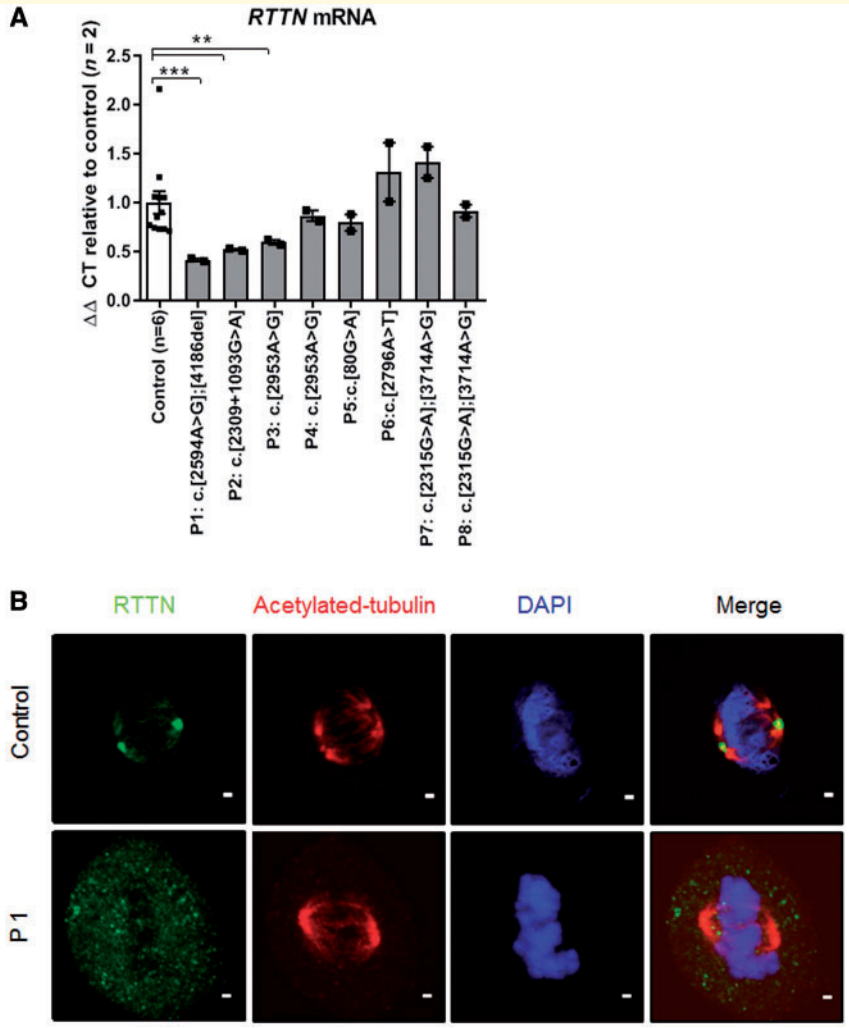

Figure 2 Expression of *RTTN* and localization of rotatin protein in human fibroblasts of affected individuals compared to healthy controls. (**A**) Quantitative PCR of *RTTN* mRNA expression shows that *RTTN* is significantly lower expressed in P1–P3. *CLK2* and *RNF111* were used as reference genes. Data are represented as the mean ± standard error of mean (SEM). Statistical two-tailed unpaired *t*-tests were performed with Welch's correction (***P = 0.0004, **P = 0.0017 for P2 and **P = 0.0055 for P3). (**B**) Fluorescent confocal imaging of human fibroblast metaphases from a representative control and P1. Antibodies were used for anti-human acetylated tubulin (red) to stain mitotic spindle and anti-human SASY to visualize rotatin (green), with DAPI for DNA (blue). Scale bars = 1 μm.

this individual showed a low expression of the c.4186del allele, resulting in a frameshift in exon 31 and a premature stop codon, suggesting that this transcript is subjected to nonsense-mediated mRNA decay. The other allele was expressed containing the pathogenic c.2594A>G missense variant (Supplementary Fig. 1A).

RT-PCR and Sanger sequencing of *RTTN* mRNA in the exons surrounding the c.[2309+1093G>A] splice alteration showed that the reduced *RTTN* mRNA expression of P2 consisted of both normal (wild-type) and altered transcript, containing an extra exon between exons 17 and 18 (p.[Ser770_Val771ins10*]) (Supplementary Fig. 1B). This exon was generated using the newly formed acceptor splice site at position c.2309+1095 and an existing wild-type donor splice site at position c.2309+1180. Insertion of this extra exon leads to a premature stop codon 10 amino acids after the new acceptor site. Most likely this results in nonsense-mediated mRNA decay and suggests that the transcript visualized in Fig. 2 escapes this alternative splicing and represents wild-type *RTTN*.

The *RTTN* sequence of P3 and P4 fibroblasts shares the same c.[2953A>G] splice variant. With RT-PCR, three transcripts were found, one wild-type, one lacking exon 23 (p.[Trp962_Arg985del]; most abundant) and one lacking both exons 22 and 23 (p.[Val930_Arg985del]) (Supplementary Fig. 1C). Although both families share the same variant and transcripts, mRNA levels and phenotype severity are variable (Grandone *et al.*, 2016; Cavallin *et al.*, 2018).

The other affected individuals, P5–P8, did not show a significantly decreased *RTTN* mRNA expression in their fibroblasts.

To determine rotatin protein level, specificity of a purified custom-made polyclonal rabbit anti-human rotatin antibody (so-called SASY, see Supplementary material) was tested on western blot after immunoprecipitation of overexpressed exogenous (Myc-tagged) rotatin in HEK293T cells, transfected with a vector containing full-length *RTTN* sequence (Supplementary material and Supplementary Fig. 2A) and tested with immunocytochemistry in HEK293T cells expressing exogenous rotatin (Supplementary Fig. 2B) (Kheradmand Kia *et al.*, 2012). Endogenous rotatin protein level was below detection limit on western blots in human control fibroblasts. However, the SASY antibody was sufficient to identify rotatin by immunocytochemistry in human fibroblasts, in both controls and mutants, indicating that none of the human variants abolish *RTTN* expression completely (Fig. 2B and Supplementary Fig. 2C). In control fibroblasts, as previously reported for HeLa, KE37 and U2OS cells (Stevens *et al.*, 2009; Kheradmand Kia *et al.*, 2012; Chen *et al.*, 2017), rotatin concentrated at the centrosomes during mitosis (Fig. 2B and Supplementary Fig. 2C). Interestingly, in mitoses examined in *RTTN* mutant fibroblasts, rotatin was not concentrated at the centrosomes but showed a weak and diffuse granular cytoplasmic staining, indicating that all tested variants lead to mislocalization of the protein (Supplementary Fig. 2C). This prompted us to question the effect of *RTTN* mutations on centrosome function and mitosis.

Rotatin in mitosis

RTTN mutant fibroblasts exhibit centrosome amplification

To study the effect of *RTTN* variants on centrosome function and mitosis, we systematically followed all the phases of mitosis in *RTTN* mutant cells using mitotic spindle marker acetylated tubulin, centrosome marker gamma tubulin and DNA marker DAPI. In cell lines from affected individuals, we significantly and consistently observed an increase of mitotic spindles with more than two centrosomes, starting from the prophase, leading to multipolar spindles and abnormal distribution of centrosomes during mitosis and cytokinesis. Centrosome amplification is shown in different phases of mitosis in all the cell lines with *RTTN* mutation in this cohort (Fig. 3A and Supplementary Fig. 3A–H) compared to healthy controls (Supplementary Fig. 3I), with statistical significance (10–14% multipolar divisions versus 0–1% in 10 control cells lines, Fig. 3B). When healthy human fibroblasts were treated with siRNA targeting *RTTN* mRNA, abnormal centrosome amplification was observed during all phases of cell division in 7% of the mitotic cells (Fig. 3B and C), proving that the observed multipolar spindle formation is a direct consequence of *RTTN* inactivation.

Rotatin regulates G2/M cell cycle progression and bipolar spindle formation

If a cell has more than two centrosomes during cell division, several pathways to repair bipolar spindle assembly may be activated, leading to centrosome clustering or centrosome inactivation (Marthiens *et al.*, 2012). This results in prolongation of the cell cycle (Marthiens *et al.*, 2012). When repair mechanisms are inefficient, centrosome numerical abnormalities in mitosis can lead to apoptotic cell death due to multipolar cell division creating aneuploidy or due to kinetochore-merotelic attachment errors creating chromosome instability (Marthiens *et al.*, 2012). During interphase, centrosome amplification can lead to multiple basal body and primary cilia formation, as observed in Cdk5rap2/MCPH3 mutant mouse embryonic fibroblasts (Barrera *et al.*, 2010; Marthiens *et al.*, 2012). To further determine the consequences of centrosome amplification in *RTTN* mutants, Hoechst 33342-mediated flow cytometric cell cycle analysis was performed in affected fibroblasts (Fig. 4A–F). This revealed a decrease in G1-phase and a G2/M cell cycle arrest in *RTTN* mutated cells (Fig. 4A and C). Histograms of *RTTN* mutant cell cycle also showed DNA fragmentation in sub-G1 phase, suggesting increased apoptotic cell death, compared to controls (Fig. 4D). Increase in apoptosis, often regulated by activation of p53, is a known consequence of the observed centrosome amplification since this can result in aneuploidy (Aylon and Oren, 2011; Marthiens *et al.*, 2013). Indeed, we observed a significant increase in aneuploid cells in P1

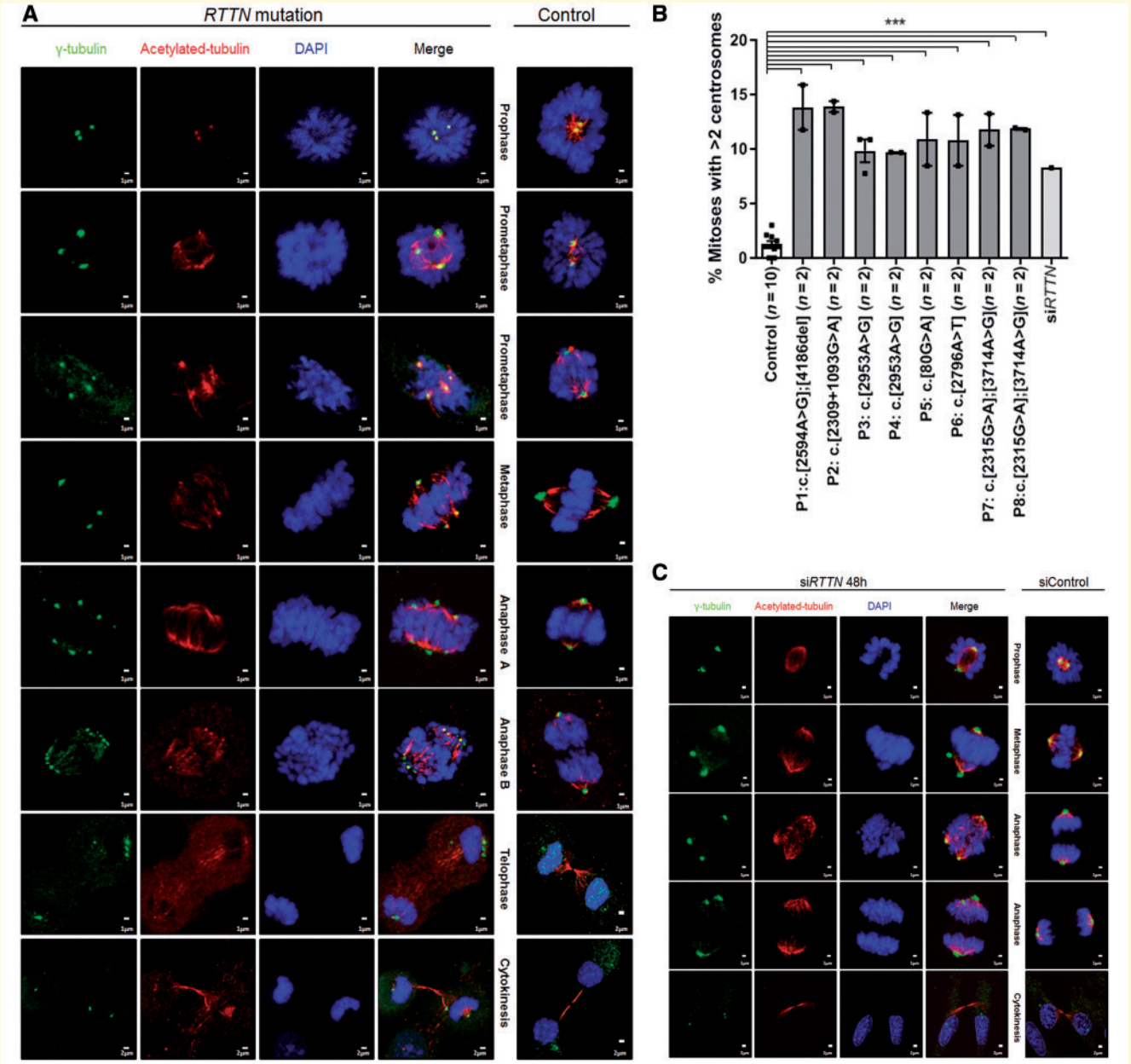

Figure 3 *RTTN* mutant fibroblasts exhibit centrosome amplification during all phases of the mitosis. (**A**) Fluorescent confocal imaging showing representative mitotic cells in all phases of cell division with more than two centrosomes in human fibroblast cells with *RTTN* mutation, compared to normal bipolar spindle formation with two centrosomes in healthy control cell lines. Antibodies used were mouse monoclonal anti-human acetylated tubulin (red), rabbit polyclonal anti-human gamma tubulin (green) and DAPI (blue). (**B**) Double-blind quantitative analysis of mitotic cells with more than two centrosomes in human fibroblast cells of all *RTTN* cases compared to healthy controls. Data are represented as the mean ± SEM. Statistical two-tailed unpaired *t*-tests were performed (***$P < 0.0001$). (**C**) Fluorescent confocal imaging of mitotic cells with more than two centrosomes in human fibroblast cells after 48 h si*RTTN* treatment indicating centrosome amplification. Antibodies used were mouse monoclonal anti-human acetylated tubulin (red), rabbit polyclonal anti-human gamma tubulin (green) and DAPI (blue).

fibroblasts (Fig. 4E). Moreover, complete knockout of *RTTN* in RPE1 cells was only viable in a $Tp53^{-/-}$ background, supporting this hypothesis (Chen *et al.*, 2017). Though *Tp53* messenger RNA and protein level were not significantly altered in the *RTTN* mutant fibroblasts (Supplementary Fig. 4A and B), differential post-translational activation of p53 could cause the increased apoptosis.

RTTN depletion not only affects the cell cycle phase distribution, ploidy and apoptosis, but also influences bipolar cell division and cell cycle duration. Real-time imaging of the fibroblasts' mitoses in healthy control cells and P1

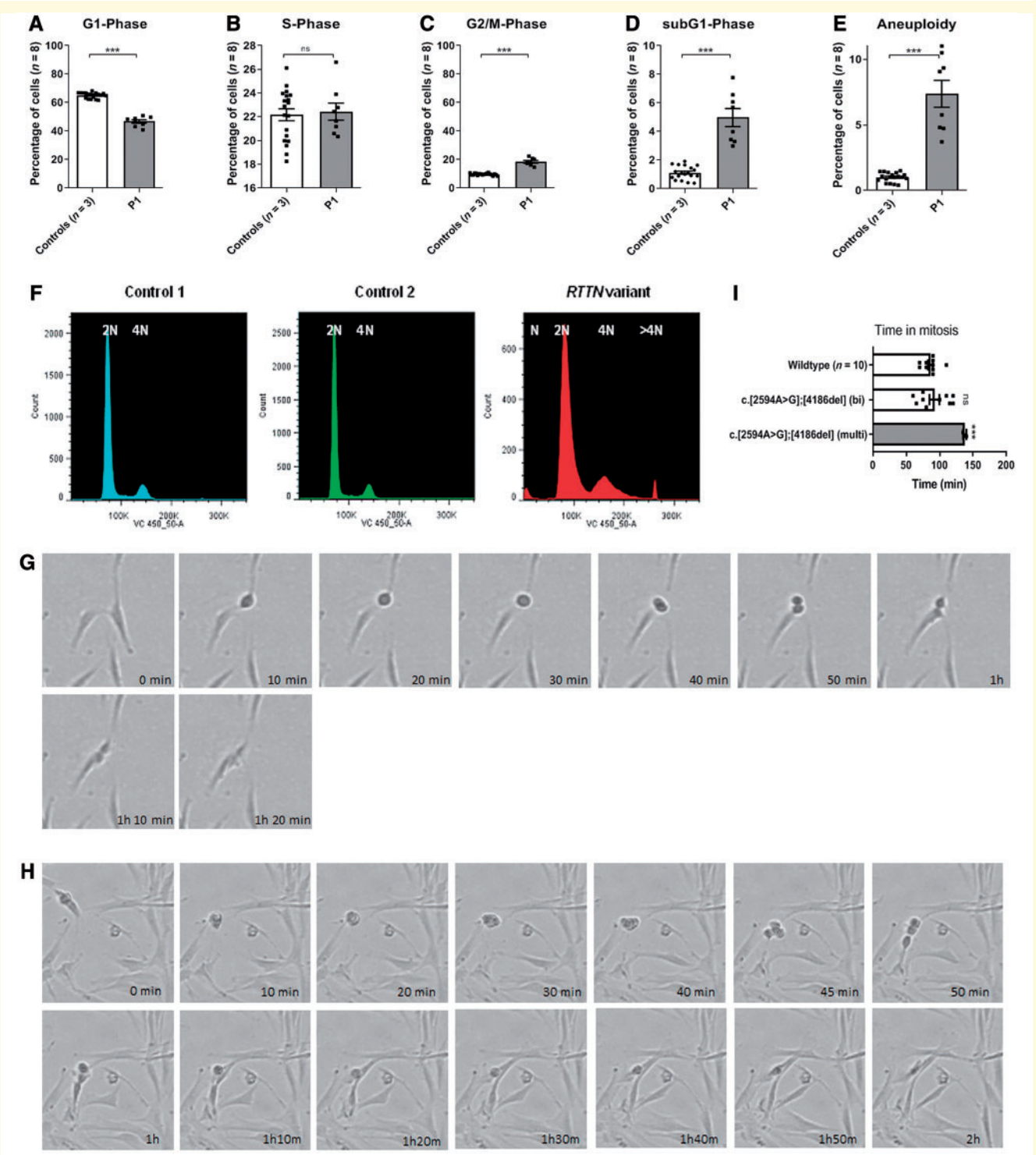

Figure 4 Rotatin in mitosis regulates G2/M cell cycle progression and bipolar spindle formation. (**A**–**F**) Flow cytometric cell cycle analysis in human fibroblasts of three healthy controls and P1 after staining with Hoechst 33342, showing percentage of fibroblasts (**A**) in G1 cell phase, (**B**) in S phase, (**C**) in G2/M phase, (**D**) in apoptotic sub-G1, (**E**) with aneuploidy (>4N) (adapted *y*-axis) and (**F**) the accompanying flow cytometry histograms of the cell lines. Analysis was performed with FlowJo 7.6.5 and statistical two-tailed unpaired *t*-tests were performed (***$P < 0.0001$). Data are represented as the mean ± SEM. (**G**–**I**) Time-lapse brightfield microscopic imaging of control and P1 human fibroblasts, showing (**G**) bipolar divisions in healthy control fibroblasts, (**H**) a tripolar division in P1, and, (**I**) an overall increase in the duration of mitosis for multipolar divisions ($n = 2$) compared to bipolar divisions ($n = 10$) (unpaired *t*-tests were performed, $P < 0.0001$). Data are represented as the mean ± SEM.

revealed that *RTTN* mutation led to tripolar/multipolar cell divisions (Fig. 4H). All control fibroblasts divided in a bipolar manner. When comparing the duration of mitosis between both cell lines by time-lapse microscopy, multipolar divisions showed a highly significant increase in duration of each cell cycle (80 min in control versus 120 min in P1 cells) (Fig. 4I). Prolonged mitosis is often observed with centrosome amplification, since the spindle assembly checkpoint network will only stimulate the cell to progress to mitosis when accurate chromosome segregation can be guaranteed (Basto *et al.*, 2008; Marthiens *et al.*, 2012). This result correlates with the flow cytometry data showing a G2/M phase arrest. If the cell has more than two centrosomes, this requires more kinetochore-microtubule interactions to stabilize the cell and favours centrosome clustering (Marthiens *et al.*, 2012). This prolongation does not always lead to correct division of the cell, and still can result in multipolar divisions (Marthiens *et al.*, 2012), as was shown in our experiment (Fig. 4H).

Rotatin in ciliogenesis and SHH signalling

Cell cycle defects in neuronal progenitors can lead to microcephaly. Individuals with *RTTN* mutations, however, not only present with primary microcephaly, but also display a broader cortical phenotype because of impaired neuronal migration and post-migrational organization. We have previously shown that cells with pathogenic *RTTN* variants build up short cilia ($<3\,\mu m$) (Kheradmand Kia *et al.*, 2012). We therefore expanded the study on the effect of *RTTN* alterations on primary cilia structure and function in patient-derived fibroblasts and performed detailed analyses of interactors with full-length rotatin protein.

We previously localized rotatin to the basal body of the primary cilium, while fibroblasts transfected with si*RTTN* displayed shorter primary cilia axonemes (Kheradmand Kia *et al.*, 2012). Here, we confirm these results in fibroblasts from additional affected individuals of this cohort (Fig. 5A–C). After serum starvation, we localized rotatin to the basal body but also to the axoneme of the primary cilium in control and *RTTN* mutant fibroblasts, suggesting dynamic localization of rotatin (Fig. 5A). Six of the eight *RTTN* mutants displayed a percentage of cilia below normal (Fig. 5C). Five of the cell lines (P2, P4, P6–P8) also showed a significant amount of short cilia ($P < 0.05$, length axoneme $<3\,\mu m$), confirming our previous observation (Fig. 5B) (Kheradmand Kia *et al.*, 2012).

SHH signalling is one of the major pathways regulated at the primary cilium and $Rttn^{-/-}$ mice exhibit clinical features reminiscent of aberrant SHH function (axial rotation defects, neural tube and left-right patterning defects) (Faisst *et al.*, 2002; Kheradmand Kia *et al.*, 2012). Mutations in microcephaly-associated genes *CDK5RAP2*, *CEP152*, *CPAP*, *KATNB1* and mouse *Stil* result in defective SHH signalling, impact cilium assembly/function, indicating that primary cilia are important for neural progenitor maintenance in the neocortex (Megraw *et al.*, 2011; Patwardhan *et al.*, 2018).

We tested SHH signalling by measuring the increase in *Gli1* mRNA expression after stimulation of the SHH pathway with purmorphamine, a SHH signalling agonist, in cultured fibroblasts from our P1 to P8 individuals and healthy controls (Supplementary Fig. 5). We observed a reproducible reduced stimulation of *Gli1* expression in some but not all *RTTN* mutant cells (P1–P3), compared to control cells. These results indicate that *RTTN* mutations can impair both structural and functional integrity of primary cilia.

Rotatin interacting proteins

Mass spectrometry was performed on immunoprecipitation assays on both exogenous full-length and endogenous rotatin to detect interacting proteins. A full-length rotatin expressing vector was transfected in HEK293T cells, presenting mitoses (medium containing foetal calf serum, no stimulation of ciliogenesis) (Supplementary material). In a first duplicate experiment, in the top list of significant interactors with exogenous rotatin, appears the non-muscle cellular heavy chain myosin complex (NMHC), consisting of three isoforms myosin-9 (MYH9), myosin-10 (MYH10) and myosin-14 (MYH14) (Samples 1 and 2 in Supplementary Table 4 and Experiment 1 in Supplementary Table 5), mitochondrial (respiratory chain) proteins and proteins with exquisite nuclear localization. Interestingly, the neuronal isoform myosin 10 presented with the highest enrichment ratio (Experiment 1 in Supplementary Table 5). In repeat experiments, NMHC subunits were again detected, albeit not on top of the list, after pull down of both endogenous and exogenous (Myc-tagged) rotatin (Supplementary Tables 5 and 6). Background levels of MYH10 were determined based on immunoprecipitation of empty Myc-tagged beads with and without transfection of empty vector. Although some immunoprecipitated rotatin samples showed weaker interaction with MYH10, the number of unique peptides was still higher than in these negative controls. Moreover, liquid chromatography/mass spectrometry after immunoprecipitation of endogenous rotatin showed high and consistent interaction with unconventional myosin-18A (MYO18A), which is highly expressed in neurons and known to co-assemble with non-muscle cellular heavy chain myosins into mixed bipolar filaments (Billington *et al.*, 2015) (Supplementary Table 6). Because MYH10 is the neuronal isoform, specific binding of rotatin with MYH10 was reciprocally confirmed on western blot after immunoprecipitation of endogenous MYH10 in HEK293 cells transfected with the RTTN-Myc vector (Supplementary Fig. 6). The interaction was confirmed after mass spectrometry of pulled down endogenous rotatin using SASY antibody and detection of MYH10 (Supplementary Table 6) (Juanes-Garcia *et al.*, 2015). In skin fibroblasts, immunoprecipitation of

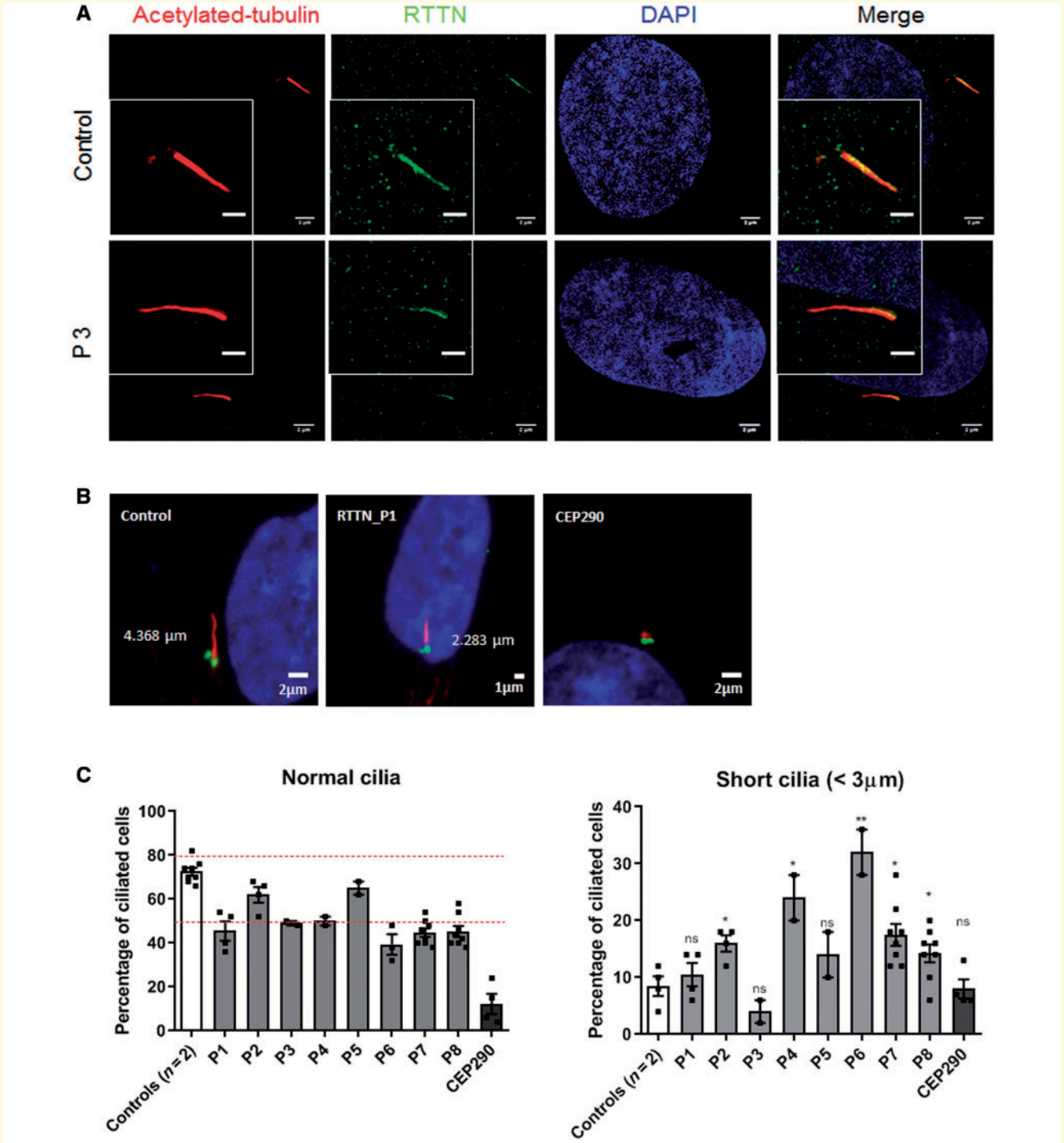

Figure 5 Rotatin in ciliogenesis. (**A**) Fluorescent 3D-SIM microscopy showing rotatin localization (green) at the basal body and axoneme during ciliogenesis 48 h after serum starvation of human control fibroblast cells and only at the axoneme in a representative *RTTN* mutant cell line. Antibodies were used for anti-human acetylated tubulin (red) to stain the axoneme and anti-human SASY to visualize rotatin (green), with DAPI for DNA (blue). Scale bars of the enlarged primary cilia represent 1 µm. (**B**) Primary cilium axoneme staining with anti-human acetylated tubulin (red) and basal body staining with anti-human γ-tubulin (green) in human fibroblasts of one control human cell line, one representative *RTTN* mutant P1 and one *CEP290* mutant cell line, with a compound heterozygous variant c.[1501G>T];[4522C>T], p.[Glu501*];[Arg1508*], showing shorter cilia in *RTTN* mutants and *CEP290* ciliopathy control. (**C**) Percentage of normal and short (<3 µm) cilia in all cell lines after initiation of ciliogenesis through 48 h of serum starvation (0.5% foetal calf serum), showing significant lower number of normal cilia and increase of shorter cilia in multiple individuals with *RTTN* mutation (statistical two-tailed unpaired *t*-tests, $^{**}P < 0.005$ $^{*}P < 0.05$). The normal range for ciliation (50–80%) is shown by dashed red lines and was determined from ∼100 experiments using several different control fibroblast lines. As a positive ciliopathy control we used the human *CEP290* mutant cell line, showing 12% of normal cilia and 8% of short cilia with a total of 20% ciliated cells. Values indicate average ± SEM for separate duplicate or quadruplicate experiments.

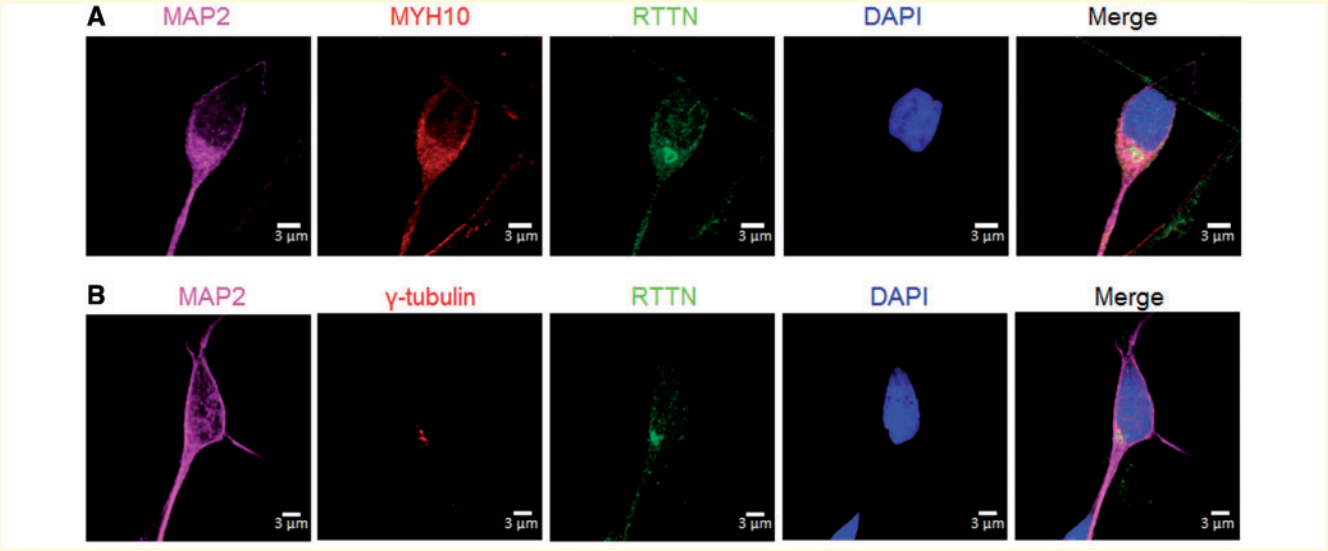

Figure 6 Rotatin localization in human iPSC-derived neurons. (**A**) Endogenous rotatin (green, rabbit anti-human RTTN SASY antibody) localized at the leading edge of the neuron, together with MYH10 at the proximal end of the leading process (red, mouse monoclonal anti- human non-muscle myosin IIB antibody). Neuronal marker major microtubule associated protein (MAP2) was stained in magenta to confirm neuronal identity with guinea pig polyclonal anti-human MAP2. (**B**) Endogenous rotatin (green) co-localized with centrosome marker γ-tubulin (red). Nuclei are visualized with DAPI (blue).

rotatin revealed co-precipitation of MYH10, confirming this interaction although no clear-cut difference could be appreciated between controls and cells from affected individuals (Supplementary Fig. 7). Among structural centrosomal proteins, CETN2 (centrin 2) showed a significant enrichment ratio in experiments with exogenous rotatin (Experiments 1 and 2 in Supplementary Table 5). Mass spectrometry of endogenous rotatin did show binding with other centrosomal/basal body proteins PCNT (pericentrin), BBS1 and BBS7 (Bardet-Biedl syndrome 1 and 7), CEP97 (Supplementary Table 6), and consistent interaction with TUBB3 and TUBB6 beta chain tubulin, which are microtubule associated proteins necessary for cell division, neuronal migration and *TUBB3* mutations have been associated with cortical malformations (Supplementary Table 6) (Bahi-Buisson and Cavallin, 2016).

Rotatin in neuronal migration

Migration of bipolar neuronal progenitors along a radial glial scaffold is essential for the proper lamination of the cortex and is regulated by a two-step process. First, the centrosome and Golgi apparatus are migrating from the perinuclear zone into the leading edge of the migrating neuron. Secondly, the forward nuclear movements are orchestrated by the perinuclear microtubule cage, anchored to the centrosome, and the actomyosin cytoskeleton (nuclear translocation or nucleokinesis) (Bellion *et al.*, 2005). Alterations in genes regulating these individual steps, are known to lead to malformation of cortical development e.g. *LIS1*, dynein and *DCX*. Human induced pluripotent stem cell (iPSC)-derived mixed neuronal cultures containing radial glial-like progenitors can recapitulate migrating bipolar neurons and have been instrumental to show migration defects in cells with *LIS1* mutations (Bamba *et al.*, 2017). We studied the expression of rotatin in human iPSC-derived neuronal cultures generated from healthy control fibroblasts according to Quadri *et al.* (2018). These cultures contain mature differentiated neuronal lineages (MAP2- and beta tubulin III-positive staining), mixed with mature radial glial cells (GFAP- and vimentin-positive) (Fig. 6A, B and Supplementary Fig. 8) and have been shown to contain both dopaminergic and glutamatergic lineages (Reinhardt *et al.*, 2013; Quadri *et al.*, 2018). Some of these cells assume a bipolar structure typical of migrating neurons, with a clearly recognizable leading edge, as deduced by the position staining of the leading centrosome (γ-tubulin-positive) (Fig. 6B). Rotatin localization was polarized with γ-tubulin at the neuronal leading edge (Fig. 6B). MYH10 was also detected in the perikaryon, predominantly at the leading edge of the migrating neurons, corresponding to its previously established role in nuclear dynamics and co-localizing with rotatin (Fig. 6A).

Discussion

Clinical phenotype

In this manuscript we reviewed the phenotypic characteristics observed in all previously published and novel individuals ($n = 28$) with *RTTN* mutations.

The emerging global phenotype is heterogeneous, and confirm the original description of two apparently separate

clinical entities: at the milder end of the spectrum a neurodevelopmental delay syndrome, near normal growth with a polymicrogyria-like cortical malformation and, at the severe end, a microcephalic primordial dwarfism (MPD) with different types of cortical malformation (Fig. 1 and Table 1) (Kheradmand Kia *et al.*, 2012; Shamseldin *et al.*, 2015). In this spectrum, the neurological problems predominate in the clinical course, including severe cognitive, motor and speech delay and only rarely seizures (17% of total). The *Rttn* knockout mouse model (Faisst *et al.*, 2002) and the *Nt* natural rotatin mutant (Chatterjee *et al.*, 2007) are associated with embryonic heart looping defects and failure to undergo axial rotation, the earliest events determining mammalian left-right asymmetry. In the human *RTTN* case series, the malformations of internal organs are less prominent and mostly not fatal. Review of all the cases shows low but consistent frequency of internal organ malformations, most frequently of the renal/urogenital system (~40%) within the MPD phenotype. The cause of early death has been cerebral dysgenesis in three of four cases (Shamseldin *et al.*, 2015; Rump *et al.*, 2016; Wambach *et al.*, 2018) and complications of congenital heart disease in one of four (Shamseldin *et al.*, 2015; Rump *et al.*, 2016; Wambach *et al.*, 2018) (Table 1 and Supplementary Table 2). The malformations of internal organs are compatible with cilia abnormalities, i.e. SHH pathway defects, but the relatively low frequency might relate to the sufficient residual rotatin protein function in most individuals. Interesting is the occurrence of severe dermatitis in few individuals (17%) reminiscent of skin rashes in DNA repair disorders and Warsaw breakage syndrome (Bailey *et al.*, 2015). Common survival into adulthood suggests lack of neurodegeneration, a typical mechanism in MPD from DNA repair defects.

About 81% of the individuals are microcephalic at birth and in total 86% (24 of 28 patients) have microcephaly at follow-up, which means that lack of microcephaly at birth is not an exclusion criterion for *RTTN* mutations (Table 1). However, primordial dwarfism, which can co-occur with primary microcephaly, is not obligatory in all microcephalic subjects. The cortical malformations can be ascribed to proliferation (simplified gyri), migration (lissencephaly, heterotopia) and organization (polymicrogyria-like dysgyria) defects of the cortex, with predominance for underdevelopment of the frontal telencephalon. The hindbrain is usually spared. Abnormalities of the ventral telencephalon might occur in some individuals with suspected mild frontal lobar holoprosencephaly and fusion of basal ganglia (Supplementary Table 2, P3) (Shamseldin *et al.*, 2015; Cavallin *et al.*, 2018), hypoplastic olfactory bulb and rostrum of the corpus callosum, hypotelorism and eye maldevelopment. Remarkably, many severely affected subjects show large interhemispheric cysts (Grandone *et al.*, 2016) (Family I and Fig. 1O and P), sometimes with severe brain disruption, a phenomenon that might relate to the hydrocephaly of $Rttn^{-/-}$ knockout mice (Faisst *et al.*, 2002).

Genotype–phenotype correlation

Review of all reported mutations shows that the variants are not restricted to specific areas or putative rotatin functional domains and they do not cluster with phenotypes (Fig. 1Q and Supplementary Table 2). The recurrent homozygous variant c.2953A>G has now been reported in three unrelated families (Families C, D and H) from Morocco, presenting with MPD and severe intellectual disability in all, suggesting that it is a founder mutation in the Moroccan population. However, no haplotype analysis has been reported in support. Four (deep) intronic mutations have an important phenotypic effect (Fig. 1Q), indicating that diagnostic tests should include these four along with careful analysis of *RTTN* non-coding regions. Indeed, homozygous intronic splicing variants in *RTTN* (premature stop) led to primary microcephaly and primordial dwarfism with a less severe outcome, a prolonged survival with a stable non-progressive course, no epilepsy and no prenatal/infant lethality (c.[2885+8A>G] and c.[2309+1093G>A], $n = 2$ families), likely due to the expression of residual wild-type transcript (Fig. 2A) (Family B and Shamseldin *et al.*, 2015). However, a compound heterozygous mutation with an intronic mutation in one allele and an exonic missense in the other, led to refractory epilepsy and dead in infant stage (c.32–3C>T) (Wambach *et al.*, 2018) and the combination of an intronic mutation with a premature stop in an exon (c.[3705C>A];[4748–19T>A] (Family I in Supplementary Table 2) even led to terminated pregnancies with intrauterine growth restriction, microcephaly, insufficient cerebral sulcation, large posterior interhemispheric cyst and cerebral schizencephalic clefts. Hence, in case only one exonic *RTTN* mutation is detected and the patient phenotype is as severe as described in these latter cases, the presence of a (deep) intronic mutation in the other allele should be considered. Moreover, when a stable non-progressive course of the MPD phenotype is observed, a homozygous intronic *RTTN* mutation should be considered. Three of the four depicted intronic mutations were picked up with whole exome sequencing, but the deep intronic mutation c.[2309+1093G>A] is only detectable with whole genome sequencing (WGS). Therefore, an alternative to WGS, this deep intronic variant should be screened separately.

Interestingly, even the same homozygous *RTTN* mutation can lead to a variable phenotype, e.g. P3 (Family C) does not exhibit skin, cardiac and genital abnormalities, as was described for two siblings with the same c.2953A>G homozygous variant (P4, Family D) (Grandone *et al.*, 2016; Cavallin *et al.*, 2018). Moreover, P3 (Family C) also has suspected holoprosencephaly, which was not present in Family D. Quantification of *RTTN* mRNA with qPCR shows residual transcripts in all affected individuals, including those who died prematurely, suggesting that complete lack of *RTTN* mRNA is probably embryonically lethal in human, as seen in $Rttn^{-/-}$ knockout mice (Faisst *et al.*, 2002). A clear genotype–phenotype correlation is lacking

for the known *RTTN* mutations. One possible explanation is that this large protein (2226 amino acids) has many protein interaction domains and interacts differently during the phases of the cell cycle. So, the individual genetic make-up could be an important determinant of the phenotype. However, a link could be made between the amount of *RTTN* wild-type mRNA expression and phenotypic severity. Three individuals in our cohort displayed a significant lower mRNA expression (Fig. 2A, P1–P3). Two of them, grouped among the most severely affected individuals (P1 and P3), expressed only the transcript originating from the missense allele (P1) or a combination of alternatively spliced transcript with wild-type mRNA (P3) (Fig. 2A and Supplementary Fig. 1A and C). Instead, P2, with a milder phenotype, had a reasonable expression of wild-type sequence (Fig. 2A).

Dynamics of rotatin function in the cell

To understand the phenotypic heterogeneity, we studied *RTTN* mutant fibroblasts to address the role of rotatin in different pathways of cortical development (cell proliferation, ciliogenesis and neuronal migration).

To date, almost all known MCPH-associated genes play a key role in centriole, centrosome and cell division regulation. Rotatin has been previously localized to the centrosome in HeLa, KE37 and U2OS (Stevens *et al.*, 2009; Kheradmand Kia *et al.*, 2012; Chen *et al.*, 2017), and we confirmed this localization in human fibroblasts and human iPSC-derived neurons. Interestingly, in *RTTN* mutated fibroblasts the residual protein does not localize to the centrosome during mitosis but is spread rather diffusely over the cytoplasm. The absence of rotatin in centrosomes leads to centrosome amplification during mitosis in all cell lines bearing the mutations and si*RTTN* treated cell lines. A similar observation has been made for *D. melanogaster* homologue *Ana3* mutant neuroblasts, showing 44% of cells with centrosome amplification, and $RTTN^{-/-}/TP53^{-/-}$ knockout in RPE1 cells, showing numerous primitive procentriole bodies (Stevens *et al.*, 2010; Chen *et al.*, 2017). Variants in centrosome genes leading to supernumerary centrosomes have also been described in individuals with autosomal primary microcephaly and primordial dwarfism, caused by variants in *STIL* (Arquint and Nigg, 2014; Marthiens and Basto, 2014), *CEP135* (Hussain *et al.*, 2012), *CDK5RAP2* (Barrera *et al.*, 2010), *MCHP1* (Gambarotto and Basto, 2016) and *CDK6* (Gambarotto and Basto, 2016). Centrosome amplification in *RTTN* mutants thus seems to be a key factor in the aetiology of MCPH. Although no exact correlation could be made between the percentage of centrosome amplification and phenotypic severity, si*RTTN* showed a lower amplification percentage (7%) than *RTTN* mutants (10–14%), suggesting that residual wild-type rotatin contributed to normal centrosome duplication. Moreover, patients with the same *RTTN* mutation (P3 and P4, P7 and P8) displayed the same percentages of centrosome amplification.

We questioned the consequences of the observed centrosome amplification and how this could lead to depletion of the neural progenitor pool during brain development. Centrosome amplification in murine neuronal stem cells is known to highly reduce brain size at birth, through multipolar cell division and formation of merotelic kinetochore attachments hindering timely chromatids segregation, eventually promoting aneuploidy (Marthiens *et al.*, 2013). Aneuploid neuronal stem cells can either enter apoptosis or prematurely differentiate to neurons, overall depleting the neuronal stem cell population at the ependymal ventricular zone (Marthiens *et al.*, 2013). Live imaging of mitoses in *RTTN* mutated fibroblasts uncovered that centrosome amplification induced multipolar cell divisions. When studying cell cycle distribution in *RTTN* mutants more extensively with flow cytometry, we observed significant increase in aneuploid cells (>4N) and consequent increase in DNA fragmentation (sub-G1 fraction), indicating apoptotic cell death. *RTTN* mutation also resulted in fewer cells entering G1-phase, G2/M cell cycle arrest and a prolonged cell cycle. At this point, the process leading to the observed centrosome amplification due to *RTTN* mutation is unclear. It is known that centrosome amplification can either result from a DNA damage induced G2/M phase arrest, which is observed when DNA damage response genes are implicated (*MCPH1*, and Seckel syndrome associated *ATR/ATM*), or it can result directly from a defect in cell division (tetraploidization) or in centrosome duplication (Krämer, 2009; Megraw *et al.*, 2011; Godinho and Pellman, 2014; Gambarotto and Basto, 2016). In analogy with *D. melanogaster* homologue *Ana3* mutant neuroblasts, centrosome amplification in *RTTN* mutants might be caused by centrosome missegregation due to failure in pericentriolar matrix recruitment (Stevens *et al.*, 2009). Indeed, rotatin has been shown to be involved in recruitment to the centrosome of CEP295 (Ana1 in *D. melanogaster*), necessary for stabilization of the centrioles to become competent for duplication (Chen *et al.*, 2017). Whether the observed G2/M phase arrest in *RTTN* mutants is the cause rather than the consequence of the observed centrosome amplification and cell death remains to be elucidated. It would be interesting to study the role of *RTTN* in DNA damage response, especially since some clinical features are similar to Seckel syndrome, and proteomics results of endogenous rotatin showed high interaction with key regulators in DNA damage response, e.g. CNOT1 (CCR4-NOT transcription complex subunit 1), downstream ATM/ATR-pathway proteins PSME3 and SIRT1 inhibitor CCAR2/DBC1, E3 SUMO-protein ligase RANBP2 and E3 ubiquitin-protein ligase HERC2. Overall, our study of cell cycle suggests that microcephaly in *RTTN* mutants is caused by both a defective mitosis and unscheduled apoptosis of neuronal progenitors during brain development, explaining why the phenotype in some affected individuals worsened postnatally.

Rotatin has been previously implicated in ciliogenesis and localized to the basal body of the primary cilium (Stevens *et al.*, 2009; Kheradmand Kia *et al.*, 2012; Wambach *et al.*, 2018). Primary cilia of cerebral cortical progenitors and neurons are paramount during multiple steps of corticogenesis, e.g. neurogenesis, apical-basal polarity of radial glial scaffold, neuronal migration, development and connectivity (Guo *et al.*, 2015; De Mori *et al.*, 2017). We show here that six of the eight *RTTN* mutant fibroblast cell lines had a decreased number of ciliated cells and five of them had an increased number of short cilia. 3D-SIM microscopy localized rotatin not only to the basal body but also to the whole axoneme. We observed a defective stimulation of the SHH pathway in some, but not all *RTTN* mutants, potentially explaining phenotypic characteristics of the affected individuals related to *SHH* defect [P1 had tetralogy of Fallot, P3 and one individual from Shamseldin *et al.* (2015) have suspected holoprosencephaly and >65% present with midline defects]. Again, no exact correlation could be made between the structural/functional integrity of the primary cilia and the phenotype, but P1 and P3 fibroblasts showed clear defective SHH stimulation (Supplementary Fig. 5) and displayed among other patient cells a lower amount of normal ciliated cells, potentially correlating to the observed midline defects. These findings highlight the role of rotatin in ciliogenesis.

The involvement of rotatin in centriole elongation (Chen *et al.*, 2017), centrosome amplification and its localization to the axoneme, confirm the existence of interconnectivity between ciliogenesis and cell cycle progression (Izawa *et al.*, 2015). Mass spectrometry of interacting partners uncover that rotatin binds with the non-muscle cellular heavy chain myosin complex (Supplementary Tables 4, 5 and Supplementary Fig. 7). In animal models, other microcephaly associated proteins have been shown to interact with this complex, *Drosophila* Asp (ASPM homologue) interacts with Myo-II (MYH10 homologue) (Rujano *et al.*, 2013). Variants in neuronal isoform *MYH10* have been described in human and mice, leading to a *RTTN*-like phenotype with microcephaly, short stature, disorders of neuronal migration, eye and cardiac defects (observed by G.M.S.M., and Ma *et al.*, 2010; Tuzovic *et al.*, 2013; Ma and Adelstein, 2014). MYH10 is located in the vicinity of the centrioles and knockdown of *MYH10* in RPE1 cells leads to impairment of ciliogenesis, similar to what we describe for *RTTN* (Kheradmand Kia *et al.*, 2012; Hong *et al.*, 2015). Moreover, double knockdown of *Myh9* and *Myh10* in mice cardiac myocytes also showed centrosome amplification, multipolar mitotic spindle formation and increased apoptosis (Ma *et al.*, 2010). Next to a role in cell cycle, centrosome amplification and ciliogenesis, MYH10 is a key component of neuronal migration, regulating nucleokinesis (Juanes-Garcia *et al.*, 2015). Variants in *Myh10*, but also in *Aspm*, lead to mislocalization of MYH10, impairment of cell polarity and delayed nucleokinesis (Ma *et al.*, 2004; Rujano *et al.*, 2013). MYH10 localizes to the leading edge of migrating neurons, determining front–back polarization, increases actomyosin bundling in the proximal end of the leading process, and promotes somal translocation during nucleokinesis (Solecki *et al.*, 2009; Juanes-Garcia *et al.*, 2015). We localized rotatin to the leading edge of migrating human iPSC-derived neurons, together with MYH10 and γ-tubulin. Based on the mass spectrometry results, co-localization in migrating neurons and the known function of myosin-10 in neuronal migration, we hypothesize that one of the processes leading to neuronal migration defects in *RTTN* mutation could be impairment of the rotatin-myosin binding.

Co-localization of rotatin with key regulators of neuronal migration at the centrosome in the leading edge of migrating neurons, together with transient binding with myosin isoforms, centrosomal proteins and microtubules, underlines the pivotal role of rotatin in neuronal migration. Further extensive investigation in conditional animal models of neuronal migration is required to prove this hypothesis.

STIL, CEP135 and PPP1R35 have been proposed as interacting proteins of rotatin (Gupta *et al.*, 2015; Chen *et al.*, 2017; Sydor *et al.*, 2018). Our mass spectrometry results did not show binding of full-length exogenous or endogenous rotatin with STIL, CEP135 or PPP1R35, possibly explained by the transience of some interactions through the dynamic localization of rotatin during cell cycle, or the specific *RTTN* constructs used. Chen *et al.* (2017) showed that the truncated N-terminal of exogenous rotatin (amino acids 1–889) binds with the N-terminal of exogenous STIL, and that a defective binding with this protein could explain the microcephalic phenotype in one of the four studied *RTTN* variants (Chen *et al.*, 2017). However, not all *RTTN* cases, in this cohort and published elsewhere, bear variants in this N-terminal domain, indicating that STIL is not the only mediator of rotatin function.

In conclusion, *RTTN* mutations lead to a complex and heterogeneous human disease phenotype. We show that rotatin is a dynamic protein involved in cell cycle progression and mitosis, in ciliogenesis and in neuronal migration, providing clues to explain the different phenotypes and confirming its central role within the dynamic network of centrosomal proteins (Jakobsen *et al.*, 2011).

Web resources

dbSNP https://www.ncbi.nlm.nih.gov/SNP/
ESP http://evs.gs.washington.edu/EVS/
ExAc database http://exac.broadinstitute.org
GoNL http://www.nlgenome.nl/
gnomAD database http://gnomad.broadinstitute.org
OMIM https://www.omim.org/

Acknowledgements

We thank the families for participating in this study. We thank Dr Mehrnaz Ghazvini of the Erasmus MC iPS Core Facility for differentiation of hiPSC from skin fibroblasts (ID EMC20i/cao388) and Professor Vincenzo Bonifati and Dr. Wim Mandemakers for advice on human iPSC-derived neurons. We thank Dr Mark Nellist for sharing materials for IP experiments. We thank Dr Charles-Joris Roux for providing MRI scans.

Funding

L.V. was supported by Steunfonds Marguerite-Marie Delacroix, Research Foundation Flanders (FWO travelgrant V429317N) and COST Action CA16118 (STSM 39032). M.W., N.B.B., A.J., R.O., W.B.D., G.M.S.M. are members of the European Network on Brain Malformations, NeuroMIG (COST Action CA16118). A.J. is supported by a Senior Clinical Investigator Fellowship from the Research Foundation Flanders (FWO). G.M.S.M. is supported by the ErasmusMC Mrace Grant #104673.

Competing interests

The authors report no competing interests.

Supplementary material

Supplementary material is available at *Brain* online.

References

Arquint C, Nigg EA. STIL Microcephaly mutations interfere with APC/C-mediated degradation and cause centriole amplification. Curr Biol 2014; 24: 351–60.

Aylon Y, Oren M. p53: guardian of ploidy. Mol Oncol 2011; 5: 315–23.

Bahi-Buisson N, Cavallin M. Tubulinopathies Overview. In: Adam MP, Ardinger HH, Pagon RA, et al., editors. GeneReviews® [Internet]. Seattle, WA: University of Washington, Seattle; 2016. 19932019. Available from: https://www.ncbi.nlm.nih.gov/books/NBK350554/.

Bailey C, Fryer AE, Greenslade M. Warsaw breakage syndrome–a further report, emphasising cutaneous findings. Eur J Med Genet 2015; 58: 235–7.

Bamba Y, Kanemura Y, Okano H, Yamasaki M. Visualization of migration of human cortical neurons generated from induced pluripotent stem cells. J Neurosci Methods 2017; 289: 57–63.

Barkovich AJ, Guerrini R, Kuzniecky RI, Jackson GD, Dobyns WB. A developmental and genetic classification for malformations of cortical development: update 2012. Brain 2012; 135 (Pt 5): 1348–69.

Barrera JA, Kao L-R, Hammer RE, Seemann J, Fuchs JL, Megraw TL. CDK5RAP2 Regulates Centriole Engagement and Cohesion in Mice. Dev Cell 2010; 18: 913–26.

Basto R, Brunk K, Vinadogrova T, Peel N, Franz A, Khodjakov A, et al. Centrosome amplification can initiate tumorigenesis in flies. Cell 2008; 133: 1032–42.

Bellion A, Baudoin JP, Alvarez C, Bornens M, Metin C. Nucleokinesis in tangentially migrating neurons comprises two alternating phases: forward migration of the Golgi/centrosome associated with centrosome splitting and myosin contraction at the rear. J Neurosci 2005; 25: 5691–9.

Bettencourt-Dias M, Hildebrandt F, Pellman D, Woods G, Godinho SA. Centrosomes and cilia in human disease. Trends Genet 2011; 27: 307–15.

Billington N, Beach Jordan R, Heissler Sarah M, Remmert K, Guzik-Lendrum S, Nagy A, et al. Myosin 18A coassembles with nonmuscle myosin 2 to form mixed bipolar filaments. Curr Biol 2015; 25: 942–8.

Cavallin M, Bery A, Maillard C, Salomon LJ, Bole C, Reilly ML, et al. Recurrent RTTN mutation leading to severe microcephaly, polymicrogyria and growth restriction. Eur J Med Genet 2018; 61: 755–8.

Chartier S, Alby C, Boutaud L, Thomas S, Elkhartoufi N, Martinovic J, et al. A neuropathological study of novel RTTN gene mutations causing a familial microcephaly with simplified gyral pattern. Birth Defects Res 2018; 110: 598–602.

Chatterjee B, Richards K, Bucan M, Lo C. Nt mutation causing laterality defects associated with deletion of rotatin. Mamm Genome 2007; 18: 310–5.

Chen HY, Wu CT, Tang CC, Lin YN, Wang WJ, Tang TK. Human microcephaly protein RTTN interacts with STIL and is required to build full-length centrioles. Nat Commun 2017; 8: 247.

De Mori R, Romani M, D'Arrigo S, Zaki MS, Lorefice E, Tardivo S, et al. Hypomorphic recessive variants in SUFU impair the sonic hedgehog pathway and cause joubert syndrome with cranio-facial and skeletal defects. Am J Hum Genet 2017; 101: 552–63.

Faheem M, Naseer MI, Rasool M, Chaudhary AG, Kumosani TA, Ilyas AM, et al. Molecular genetics of human primary microcephaly: an overview. BMC Med Genom 2015; 8 (Suppl 1): S4-S.

Deutsch EW, Csordas A, Sun Z, Jarnuczak A, Perez-Riverol Y, Ternent T, et al. The ProteomeXchange Consortium in 2017: supporting the cultural change in proteomics public data deposition. Nucleic Acids Res 2017; 54: D1100–6.

Faisst AM, Alvarez-Bolado G, Treichel D, Gruss P. Rotatin is a novel gene required for axial rotation and left-right specification in mouse embryos. Mech Dev 2002; 113: 15–28.

Gambarotto D, Basto R. Consequences of numerical centrosome defects in development and disease. In: Lüders J, editor. The Microtubule Cytoskeleton: Organisation, Function and Role in Disease. Vienna: Springer Vienna; 2016. p. 117–49.

Godinho SA, Pellman D. Causes and consequences of centrosome abnormalities in cancer. Philos Trans R Soc Lond B Biol Sci 2014; 369.

Grandone A, Torella A, Santoro C, Giugliano T, Del Vecchio Blanco F, Mutarelli M, et al. Expanding the phenotype of RTTN variations: a new family with primary microcephaly, severe growth failure, brain malformations and dermatitis. Clin Genet 2016; 90: 445–50.

Guemez-Gamboa A, Coufal NG, Gleeson JG. Primary cilia in the developing and mature brain. Neuron 2014; 82: 511–21.

Guerrini R, Dobyns WB. Malformations of cortical development: clinical features and genetic causes. Lancet Neurol 2014; 13: 710–26.

Guo J, Higginbotham H, Li J, Nichols J, Hirt J, Ghukasyan V, et al. Developmental disruptions underlying brain abnormalities in ciliopathies. Nat Commun 2015; 6: 7857.

Gupta GD, Coyaud E, Goncalves J, Mojarad BA, Liu Y, Wu Q, et al. A dynamic protein interaction landscape of the human centrosome-cilium interface. Cell 2015; 163: 1484–99.

Hong H, Kim J, Kim J. Myosin heavy chain 10 (MYH10) is required for centriole migration during the biogenesis of primary cilia. Biochem Biophys Res Commun 2015; 461: 180–5.

Hussain MS, Baig SM, Neumann S, Nurnberg G, Farooq M, Ahmad I, et al. A truncating mutation of CEP135 causes primary microcephaly and disturbed centrosomal function. Am J Hum Genet 2012; 90: 871–8.

Izawa I, Goto H, Kasahara K, Inagaki M. Current topics of functional links between primary cilia and cell cycle. Cilia 2015; 4: 12.

Jakobsen L, Vanselow K, Skogs M, Toyoda Y, Lundberg E, Poser I, et al. Novel asymmetrically localizing components of human centrosomes identified by complementary proteomics methods. EMBO J 2011; 30: 1520–35.

Juanes-Garcia A, Chapman JR, Aguilar-Cuenca R, Delgado-Arevalo C, Hodges J, Whitmore LA, et al. A regulatory motif in nonmuscle myosin II-B regulates its role in migratory front-back polarity. J Cell Biol 2015; 209: 23–32.

Kheradmand Kia S, Verbeek E, Engelen E, Schot R, Poot RA, de Coo IF, et al. RTTN mutations link primary cilia function to organization of the human cerebral cortex. Am J Hum Genet 2012; 91: 533–40.

Krämer A. Centrosomes in checkpoint responses. In: Siddik ZH, editor. Checkpoint Controls and Targets in Cancer Therapy. Totowa, NJ: Humana Press; 2009. p. 53–67.

Ma X, Adelstein RS. A point mutation in Myh10 causes major defects in heart development and body wall closure. Circ Cardiovasc Genet 2014; 7: 257–65.

Ma X, Jana SS, Conti MA, Kawamoto S, Claycomb WC, Adelstein RS. Ablation of nonmuscle myosin II-B and II-C reveals a role for nonmuscle myosin II in cardiac myocyte karyokinesis. Mol Biol Cell 2010; 21: 3952–62.

Ma X, Kawamoto S, Hara Y, Adelstein RS. A point mutation in the motor domain of nonmuscle myosin II-B impairs migration of distinct groups of neurons. Mol Biol Cell 2004; 15: 2568–79.

Marthiens V, Basto R. Microcephaly: STIL(l) a tale of too many centrosomes. Curr Biol 2014; 24: R162–4.

Marthiens V, Piel M, Basto R. Never tear us apart–the importance of centrosome clustering. J Cell Sci 2012; 125 (Pt 14): 3281–92.

Marthiens V, Rujano MA, Pennetier C, Tessier S, Paul-Gilloteaux P, Basto R. Centrosome amplification causes microcephaly. Nat Cell Biol 2013; 15: 731–40.

Megraw TL, Sharkey JT, Nowakowski RS. Cdk5rap2 exposes the centrosomal root of microcephaly syndromes. Trends Cell Biol 2011; 21: 470–80.

Patwardhan D, Mani S, Passemard S, Gressens P, El Ghouzzi V. STIL balancing primary microcephaly and cancer. Cell Death Dis 2018; 9: 65.

Quadri M, Mandemakers W, Grochowska MM, Masius R, Geut H, Fabrizio E, et al. LRP10 genetic variants in familial Parkinson's disease and dementia with Lewy bodies: a genome-wide linkage and sequencing study. Lancet Neurol 2018; 17: 597–608.

Reinhardt P, Glatza M, Hemmer K, Tsytsyura Y, Thiel CS, Hoing S, et al. Derivation and expansion using only small molecules of human neural progenitors for neurodegenerative disease modeling. PLoS One 2013; 8: e59252.

Romero DM, Bahi-Buisson N, Francis F. Genetics and mechanisms leading to human cortical malformations. Semin Cell Dev Biol 2018; 76: 33–75.

Rujano MA, Sanchez-Pulido L, Pennetier C, le Dez G, Basto R. The microcephaly protein Asp regulates neuroepithelium morphogenesis by controlling the spatial distribution of myosin II. Nat Cell Biol 2013; 15: 1294–306.

Rump P, Jazayeri O, van Dijk-Bos KK, Johansson LF, van Essen AJ, Verheij JB, et al. Whole-exome sequencing is a powerful approach for establishing the etiological diagnosis in patients with intellectual disability and microcephaly. BMC Med Genom 2016; 9: 7.

Shamseldin H, Alazami AM, Manning M, Hashem A, Caluseiu O, Tabarki B, et al. RTTN mutations cause primary microcephaly and primordial dwarfism in humans. Am J Hum Genet 2015; 97: 862–8.

Solecki DJ, Trivedi N, Govek EE, Kerekes RA, Gleason SS, Hatten ME. Myosin II motors and F-actin dynamics drive the coordinated movement of the centrosome and soma during CNS glial-guided neuronal migration. Neuron 2009; 63: 63–80.

Stevens NR, Dobbelaere J, Brunk K, Franz A, Raff JW. Drosophila Ana2 is a conserved centriole duplication factor. J Cell Biol 2010; 188: 313–23.

Stevens NR, Dobbelaere J, Wainman A, Gergely F, Raff JW. Ana3 is a conserved protein required for the structural integrity of centrioles and basal bodies. J Cell Biol 2009; 187: 355–63.

Stouffs K, Moortgat S, Vanderhasselt T, Vandervore L, Dica A, Mathot M, et al. Biallelic mutations in RTTN are associated with microcephaly, short stature and a wide range of brain malformations. Eur J Med Genet 2018; 61: 733–37.

Sydor AM, Coyaud E, Rovelli C, Laurent E, Liu H, Raught B, et al. PPP1R35 is a novel centrosomal protein that regulates centriole length in concert with the microcephaly protein RTTN. Elife 2018; 7(e37846).

Tuzovic L, Yu L, Zeng W, Li X, Lu H, Lu HM, et al. A human de novo mutation in MYH10 phenocopies the loss of function mutation in mice. Rare Dis 2013; 1: e26144.

Vizcaíno JA, Csordas A, del-Toro N, Dianes JA, Griss J, Lavidas I, et al. 2016 update of the PRIDE database and related tools. Nucleic Acids Res 2016; 44: D447–56.

Vora NL, Powell B, Brandt A, Strande N, Hardisty E, Gilmore K, et al. Prenatal exome sequencing in anomalous fetuses: new opportunities and challenges. Genet Med 2017; 19: 1207–16.

Wambach JA, Wegner DJ, Yang P, Shinawi M, Baldridge D, Betleja E, et al. Functional characterization of biallelic RTTN variants identified in an infant with microcephaly, simplified gyral pattern, pontocerebellar hypoplasia, and seizures. Pediatr Res 2018; 84: 435–41.